Proc. Natl. Acad. Sci. USA
Vol. 93, pp. 5368–5373, May 1996
Physiology

Near-membrane [Ca^{2+}] transients resolved using the Ca^{2+} indicator FFP18

ELAINE F. ETTER*, AKWASI MINTA†, MARTIN POENIE‡, AND FREDRIC S. FAY*

*Department of Physiology and Biomedical Imaging Group, University of Massachusetts Medical Center, 373 Plantation Street, Worcester, MA 01605; †TEFLABS, 9503 Capitol View Drive, Austin, TX 78747; and ‡Department of Zoology, 141 Patterson Laboratories, University of Texas, Austin, TX 78712

Communicated by Joseph F. Hoffman, Yale University, New Haven, CT, December 22, 1995 (received for review August 28, 1995)

ABSTRACT **Ca^{2+}-sensitive processes at cell membranes involved in contraction, secretion, and neurotransmitter release are activated *in situ* or *in vitro* by Ca^{2+} concentrations ([Ca^{2+}]) 10–100 times higher than [Ca^{2+}] measured during stimulation in intact cells. This paradox might be explained if the local [Ca^{2+}] at the cell membrane is very different from that in the rest of the cell. Soluble Ca^{2+} indicators, which indicate spatially averaged cytoplasmic [Ca^{2+}], cannot resolve these localized, near-membrane [Ca^{2+}] signals. FFP18, the newest Ca^{2+} indicator designed to selectively monitor near-membrane [Ca^{2+}], has a lower Ca^{2+} affinity and is more water soluble than previously used membrane-associating Ca^{2+} indicators. Images of the intracellular distribution of FFP18 show that >65% is located on or near the plasma membrane. [Ca^{2+}] transients recorded using FFP18 during membrane depolarization-induced Ca^{2+} influx show that near-membrane [Ca^{2+}] rises faster and reaches micromolar levels at early times when the cytoplasmic [Ca^{2+}], recorded using fura-2, has risen to only a few hundred nanomolar. High-speed series of digital images of [Ca^{2+}] show that near-membrane [Ca^{2+}], reported by FFP18, rises within 20 msec, peaks at 50–100 msec, and then declines. [Ca^{2+}] reported by fura-2 rose slowly and continuously throughout the time images were acquired. The existence of these large, rapid increases in [Ca^{2+}] directly beneath the surface membrane may explain how numerous Ca^{2+}-sensitive membrane processes are activated at times when bulk cytoplasmic [Ca^{2+}] changes are too small to activate them.**

In smooth muscle, stimulation at the cell membrane causes a transient elevation in intracellular free Ca^{2+} concentration ([Ca^{2+}]$_i$), which leads to activation of the contractile proteins. The magnitude, time course, and spatial distribution of the [Ca^{2+}]$_i$ transient are determined by Ca^{2+} influx and Ca^{2+} removal through Ca^{2+} channels and Ca^{2+} transporters distributed on the plasma membrane and membranes of the sarcoplasmic reticulum (SR) and mitochondria (1–6) and by the distribution of intracellular Ca^{2+} buffers (7, 8). These channels and transport mechanisms are, in turn, regulated by [Ca^{2+}]$_i$ near the membrane (3–5). The Ca^{2+} sensitivity of membrane processes such as Ca^{2+}-induced SR Ca^{2+} release, Na^+/Ca^{2+} exchange, Ca^{2+}-activated K^+ currents, and Ca^{2+} uptake in mitochondria, when measured *in situ* or *in vitro* (9–13), are in the 1- to 100-μM range. Yet during [Ca^{2+}]$_i$ transients that cause contraction, recorded using fura-2, [Ca^{2+}]$_i$ often remains in the nanomolar range. Such discrepancies have been interpreted to indicate that large, steep [Ca^{2+}]$_i$ gradients exist near the plasma membrane during Ca^{2+} influx (14–16). Local, high concentrations of Ca^{2+} (or other ions) can develop when Ca^{2+} influx or SR Ca^{2+} release are directed into a narrow space between closely apposed intracellular structures, such as the SR and the plasma membrane or the SR and mitochondria, where diffusion of Ca^{2+} may be restricted (17). Localized [Ca^{2+}]$_i$ (and [Na^+]$_i$) signals in restricted spaces have been postulated to explain the function of Na^+/Ca^{2+} exchange (18, 19) and the mechanism of Ca^{2+}-induced Ca^{2+} release in cardiac cells (20), and spontaneous transient outward currents in smooth muscle (21). Efforts to measure large changes in [Ca^{2+}]$_i$ near cell membranes using soluble Ca^{2+} indicators such as fura-2 or fluo-3, which indicate a spatially averaged cytoplasmic [Ca^{2+}]$_i$ (22, 23), have been largely unsuccessful, predominantly because the small fluorescence signal indicating near-membrane [Ca^{2+}]$_i$ is obscured by the larger signal indicating [Ca^{2+}]$_i$ changes in the rest of the cell.

Direct measurements of near-membrane [Ca^{2+}]$_i$ have been attempted using Ca^{2+} indicators designed to indicate [Ca^{2+}]$_i$ just beneath the membrane, but not in other regions of the cell, either by having a very low Ca^{2+} affinity or by having a lipophilic tail that localizes the indicator to the membrane. Llinas *et al.* (24) used the luminescent Ca^{2+} indicator, *n*-aequorin-J, which has a very low Ca^{2+} affinity, to demonstrate high [Ca^{2+}] domains beneath the cell membrane during neuronal transmitter release. But signals from this indicator were of low intensity, and long integration times were required to accumulate light in images; therefore, spatial and temporal resolution were diminished; the kinetics of the [Ca^{2+}]$_i$ changes could not be monitored adequately. The first membrane-associating fluorescent Ca^{2+} indicator, C_{18}-fura-2, was used to detect transient changes in [Ca^{2+}]$_i$ that had faster kinetics than [Ca^{2+}]$_i$ transients recorded using fura 2 (25). But C_{18}-fura-2, with a K_d for Ca^{2+} of 150 nM, becomes saturated and cannot detect further changes in [Ca^{2+}]$_i$ when [Ca^{2+}]$_i$ is >1 μM. In addition, C_{18}-fura-2 is so highly lipophilic that it diffuses very slowly out of the pipette into the cell; therefore, fluorescence signals are dim, and recorded [Ca^{2+}]$_i$ transients are noisy. FFP18, the most recently developed membrane-associating Ca^{2+} indicator, is improved in several ways over C_{18}-fura-2. Here we have characterized the spectral properties of FFP18 associated with cell membranes and determined its intracellular distribution. We have used FFP18 to directly measure changes in near-membrane [Ca^{2+}]$_i$ that occurred due to Ca^{2+} influx through voltage-gated Ca^{2+} channels and due to Ca^{2+} release from the SR to investigate the characteristics of the localized [Ca^{2+}]$_i$ transients that regulate membrane processes in smooth muscle cells.

METHODS

Smooth muscle cells were enzymatically isolated from stomachs of the toad *Bufo marinus* according to described procedures (26).

Measuring Spectral Properties. Excitation spectra of membrane-associated FFP18 at various [Ca^{2+}] were recorded using a SPEX spectrofluorimeter. Emission was collected at 510 nm. FFP18 was applied to the external surface of cells by 10- to 30-min incubations in amphibian physiological saline (APS) containing 0.5–10 μM FFP18. Cell suspensions with different free [Ca^{2+}] levels were produced by a described procedure (25). The concentration of membrane-associated FFP18 and the density of FFP18 molecules on the cell membrane were estimated using described methods (25).

The publication costs of this article were defrayed in part by page charge payment. This article must therefore be hereby marked "*advertisement*" in accordance with 18 U.S.C. §1734 solely to indicate this fact.

Abbreviations: SR, sarcoplasmic reticulum; [Ca^{+2}]$_i$, intracellular free Ca^{2+} concentration; APS, amphibian physiological saline.

Measuring Membrane Current and $[Ca^{2+}]_i$. Isolated smooth muscle cells were voltage-clamped using the patch-clamp technique in whole-cell configuration, and membrane currents were recorded with an Axopatch model 1D amplifier. Solutions were designed to block K^+ currents and enhance Ca^{2+} currents. Extracellular APS contained 102 mM NaCl, 3 mM KCl, 10 mM tetraethylammonium chloride, 10 mM $CaCl_2$, 1 mM $MgCl_2$, 5 mM Hepes (pH 7.4). Pipette solution contained 130 mM CsCl, 3 mM Na_2-ATP, 4 mM $MgCl_2$, 20 mM Hepes, and 15–30 μM FFP18 or 50 μM fura-2 (pH 7.1). FFP18 was obtained initially as described by Vorndran *et al.* (34) and later from TEFLABS. Ca^{2+} indicators diffused into the cell from the patch pipette. $[Ca^{2+}]_i$ transients were recorded from a small region of the cell using a microspectrofluorimeter apparatus (27). $[Ca^{2+}]_i$ was calculated from the ratio of background-corrected fluorescence at 340 and 380 nm (28).

Calibration parameters {R_{max} = fluorescence excited at 340 nm (F_{340})/F_{380} in saturating $[Ca^{2+}]$ and $R_{min} = F_{340}/F_{380}$ in absence of Ca^{2+}} for FFP18 inside patch-clamped cells were measured by permeabilizing the cell membrane with hyperpolarizations to −250 mV or brief treatments with β-escin, first in 5 mM Ca^{2+} APS to measure R_{max} and then in 5 mM BAPTA [bis(2-aminophenoxy)ethane-*N*,*N*,*N*′,*N*′-tetraacetate] APS bath solution to measure R_{min}. We could not obtain a value for β ($\beta = F_{380}$ in absence of Ca^{2+}/F_{380} in saturating Ca^{2+}) inside cells using these methods as FFP18 continuously entered the cell from the patch pipette. We found that FFP18 (0.5–15 μM) in 0.2% Triton-X 100 solutions has a dynamic range, brightness, and calibration constants more similar to membrane-associated FFP18 than to FFP18 alone in solution. Also, R_{max} and R_{min} values obtained in Triton-containing solutions were comparable to those measured for intracellular FFP18. Therefore we used R_{max}, R_{min}, and β values measured in 400 μl of Triton-containing pipette solution, which mimics the intracellular milieu. Calibration parameters for fura-2 were obtained in pipette solution without Triton-X 100.

Three-Dimensional Images. Three-dimensional images of FFP18 distribution inside single smooth muscle cells were obtained using the digital imaging microscope configured to acquire high-resolution images at multiple focal planes as described (25, 29). Isolated smooth muscle cells were patch-clamped in the whole-cell configuration. Pipette solution contained 25 μM FFP18, and extracellular APS solution contained 5 mM Ni^{2+} to quench any FFP18 in the bath or on the cell exterior. Fluorescence was excited at a wavelength (364 nm) where FFP18 is relatively insensitive to Ca^{2+}; therefore fluorescence in the images represents distribution of the indicator. A set of images at 30 focal planes across the cell, 0.5 μm apart, was acquired and then restored using a constrained, iterative deconvolution algorithm to reverse distortions caused by the optics by returning out-of-focus light to its point of origin (30).

Imaging Changes in $[Ca^{2+}]_i$. The high-speed digital imaging microscope was configured with the following features (ref. 31; see figure 1 in ref. 31). The UV lines of an Argon ion laser were split, band-pass-filtered into separately shuttered 351-nm and 380-nm beams, recombined, and used to epi-illuminate the cell through a ×100, 1.3 numerical aperture objective. Emitted fluorescence was imaged onto a charge-coupled device (CCD) camera. A mask placed at an intermediate image plane limited image-field size on the CCD to 25 × 512 pixels (corresponding to 3 μm × 61 μm of the cell). The masked area of the CCD was used to store earlier images, which were shifted into the masked region between exposures. In this configuration we could rapidly acquire 20 images (10 ratio pairs) before reading out the CCD chip, which at the 12-bit precision attained required 6 sec. To image changes in $[Ca^{2+}]_i$ in smooth muscle cells, one pair of images of intracellular fluorescence at a central focal plane was acquired before membrane depolarization using sequential 5-msec exposures at 351 nm and 380 nm separated by 2 msec. Nine more pairs of images were acquired during membrane depolarization with 10 msec between pairs. Images were dark current-subtracted and background-subtracted. Images of FFP18 fluorescence were corrected for bleaching, which was measured in series of images taken of unstimulated FFP18-loaded cells. (During a series of 10 image pairs, the fluorescence excited at 351 nm bleached 30–40%, and fluorescence excited at 380 nm bleached 15–25%.) The corrected images at 351 nm were divided by corrected images at 380 nm to obtain ratio images. We found slight, slowly varying, spatial inhomogeneities in the illumination across the image field, caused by interaction of the coherent light with imperfections in the optical components, which differed along the light paths of the two wavelengths. Therefore, the following equation, which was simply derived from the standard ratiometric equation (28) using the fact that β and the ratio of R_{min}/R_{max}, inherent properties of the dye, are unaffected by spatial variations in the excitation at the two wavelengths, was used to calculate the $[Ca^{2+}]_i$ at each pixel:

$$[Ca^{2+}] = \frac{K_d\beta[R/R_{rest} - (R_{min}/R_{max})C]}{C - R/R_{rest}}, \quad [1]$$

where

$$C = \frac{K_d\beta + [Ca^{2+}]_{rest}}{[Ca^{2+}]_{rest} + K_d\beta(R_{min}/R_{max})} \quad [2]$$

and $R = F_{351}/F_{380}$ at each pixel in the ratio images acquired during depolarization, $R_{rest} = F_{351}/F_{380}$ at each pixel in the ratio image acquired before depolarization, R_{min}, R_{max}, and β were measured during calibration, and K_d was taken to be 400 nM. The resting $[Ca^{2+}]_i$, ($[Ca^{2+}]_{rest}$), was assumed to be uniform and was calculated from an average ratio value across the cell in the ratio image acquired before depolarization.

Mathematical Analysis. $[Ca^{2+}]_i$ transients recorded using FFP18 were mathematically decomposed into cytoplasmic and near-membrane components using the following assumptions and expressions. Previous experiments (32) have shown that the integral of the inward Ca^{2+} current, multiplied by a factor to account for the buffer capacity of the cell provides a reasonable estimate of the magnitude and time course of changes in bulk cytoplasmic $[Ca^{2+}]$, ($[Ca^{2+}]_{cyto}$).

$$[Ca^{2+}]_{cyto}(t) = \sum_{t=0}^{500ms} [(i_t dt)/(2B{\cdot}F{\cdot}V)], \quad [3]$$

where i_t is the measured inward current at each sampled point, dt is the interval between measurements of i_t (3 msec), 2 is the charge on a calcium ion, B is the measured buffer capacity of the cell (32), F is the Faraday constant, and V is the cell volume (6 pl). From this we can calculate values for the fluorescence ratio in the cytoplasm (28):

$$R^{cyto}(t) = ([Ca^{2+}]_{cyto}\, R_{max} + K_d{\cdot}\beta{\cdot}R_{min})/(K_d\,\beta + [Ca^{2+}]_{cyto}). \quad [4]$$

Images of the intracellular distribution of FFP18 showed that ≈65% of the dye is near the cell surface and 35% is in the cytoplasm. We defined a variable, K, to represent the percentage of the FFP18 fluorescent signal coming from the cytoplasm:

$$F^{cyto}(Ca^{2+}\text{-independent}) = K{\cdot}F^{observed}(Ca^{2+}\text{-independent}). \quad [5]$$

Then, using an expression that relates the amount of dye present (indicated by fluorescence excited at a Ca^{2+}-insensitive wavelength) to the fluorescence at two Ca^{2+}-sensitive wavelengths (33):

$$F(Ca^{2+}\text{-independent}) = F_{380} + \alpha F_{340}, \quad [6]$$

where α = (absolute value of F_{380} change)/(absolute value of F_{340} change) for a given $[Ca^{2+}]$ change, we derived expressions for cytoplasmic F_{340} and cytoplasmic F_{380} as functions of K, α, and R^{cyto}. Calculated F_{340} and F_{380} signals attributed to

changes in bulk cytoplasmic [Ca^{2+}] were subtracted from the measured whole-cell signals to obtain calculated near-membrane fluorescence signals:

$$F^{\text{near-membrane}} = F^{\text{observed}} - F^{\text{cyto}}, \quad [7]$$

and $F_{340}^{\text{near-membrane}}(t)$ and $F_{380}^{\text{near-membrane}}(t)$ were used to calculate an estimate of the near-membrane [Ca^{2+}] transient.

RESULTS AND DISCUSSION

FFP18 is the most recent addition to a new group of indicators designed to detect near-membrane $[Ca^{2+}]_i$. The FFP18 molecule has a 12-carbon hydrophobic tail that partitions into the cell membrane and a positively charged piperazine moiety between the tail and fura-2 moiety that aids in binding to membrane phospholipids and thereby prevents the calcium-binding portion of the indicator from being pulled into the membrane (ref. 34; for chemical structure see ref. 34). We have characterized the spectral properties of FFP18 when it is associated with the external surface of cell membranes (25). The excitation spectra of a low concentration of membrane-associated FFP18 (corresponding to 1×10^{-15} mol per cell and an estimated surface density of 1.6×10^5 molecules per μm^2), shown in Fig. 1*A*, are similar to the spectra of fura-2. The calculated calcium dissociation constant (K_d) of this low concentration of membrane-associated FFP18 is 400 nM (for method see ref. 25). One observed characteristic of lipophilic fluorescent indicators is that they aggregate in solution or when packed densely on a membrane (25, 35) and when their fluorophores come close enough to interact, they quench and are nonfluorescent (36). Thus, as a fluorescent indicator is packed more densely on the cell membrane, its brightness will decrease, and its spectral properties may be altered (28). To study the concentration-dependence of spectral properties of FFP18, batches of cells were incubated with various FFP18 concentrations; the surface density

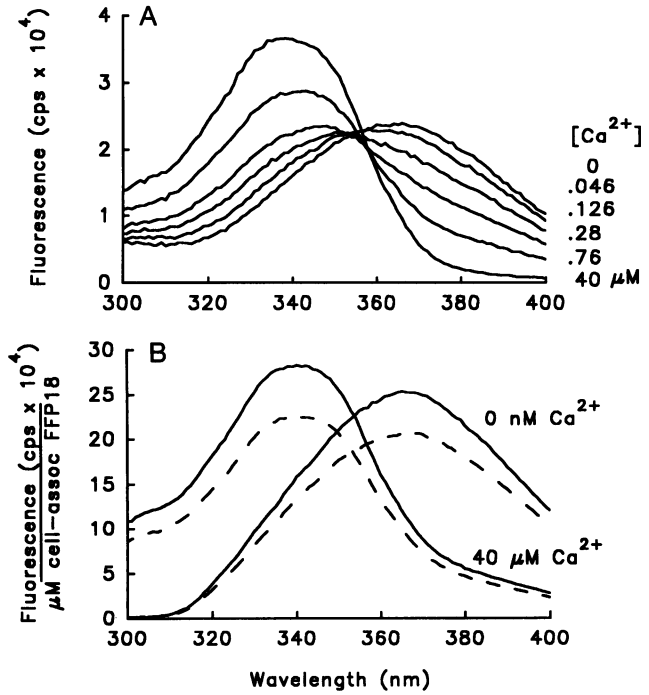

FIG. 1. Spectral properties of FFP18 associated with the external surface of cell membranes. (*A*) Excitation spectra of 0.23 μM membrane-associated FFP18 in [Ca^{2+}] ranging from 0 nM to 40 μM. Emission was collected at 510 nm. (*B*) Excitation spectra of 0.4 μM (——) and 0.95 μM (- - -) membrane-associated FFP18 in zero Ca^{2+} and 40 μM Ca^{2+}. These concentrations correspond to 2×10^{-15} and 9×10^{-15} mol per cell, respectively. Note that the fluorescence intensity is normalized by the FFP18 concentration.

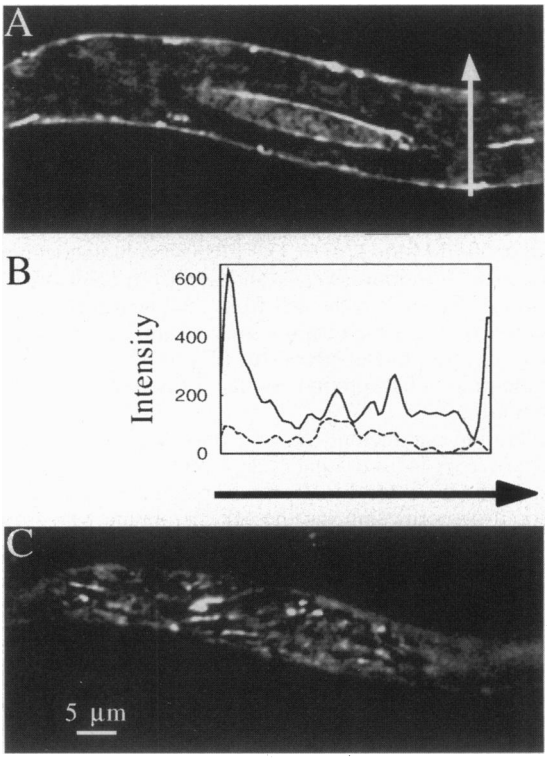

FIG. 2. Intracellular distribution of FFP18 fluorescence excited at 364 nm, where FFP18 is relatively Ca^{2+}-insensitive. (*A*) Image in a plane transecting the center of a smooth muscle cell showing the distribution of FFP18 that diffused into the cell from a patch pipette. (*B*) Plots of the fluorescence intensity along a straight line (white arrow) across the image in *A* (——) and across an image of autofluorescence in this cell (image not shown) before FFP18 was applied (- - -). (*C*) Image of FFP18 fluorescence in a plane at the cell surface.

achieved after cells were spun down and resuspended to remove excess FFP18 never exceeded 10^6 molecules per μm^2. In comparison, the surface density of C_{18}-fura-2 often reached 10^7 molecules per μm^2 after incubation with comparable dye concentrations. The lower peak packing density of FFP18 is presumably due to the extra charge or the less lipophilic tail on this molecule. Fig. 1*B* shows spectra of two concentrations (2×10^{-15} and 9×10^{-15} mol per cell corresponding to surface densities of 3.2×10^5 and 1.0×10^6 molecules per μm^2) of membrane-associated FFP18 in zero Ca^{2+} and saturating Ca^{2+}. At these higher concentrations (compared to Fig. 1*A*) the peak intensity of the spectrum in saturating Ca^{2+} is closer to the peak of the spectrum in zero Ca^{2+}. Also, as FFP18 concentration increases, the fluorescence per mol of FFP18 decreases at all wavelengths. This decrease is greater in the presence of Ca^{2+}. When FFP18 concentration was doubled, the fluorescence per mol in saturating Ca^{2+} decreased, on average ($n = 3$), twice as much as the fluorescence per mol in zero Ca^{2+}. Thus, formation of nonfluorescent aggregates occurs more readily in the presence of Ca^{2+}, presumably because Ca^{2+} binding to the tetraanionic indicator neutralizes charges that would otherwise repel other FFP18 molecules.

Because of the way the FFP18 spectrum is altered at higher membrane densities, the parameters measured to calibrate the dye also depend on dye density on the membrane. The R_{max} and β values are smaller at higher FFP18 concentrations. When the concentration of membrane-associated FFP18 on the external cell surface was doubled, over the range from 5×10^{-16} to 5×10^{-15} mol per cell, R_{max} decreased 25%, β decreased 20%, and R_{min} was constant ($n = 4$). Thus, uncertainties in calculated [Ca^{2+}] during an experiment will be minimized when the FFP18 concentration during the experiment and calibration are the same. Concentration mismatches that might have occurred in our

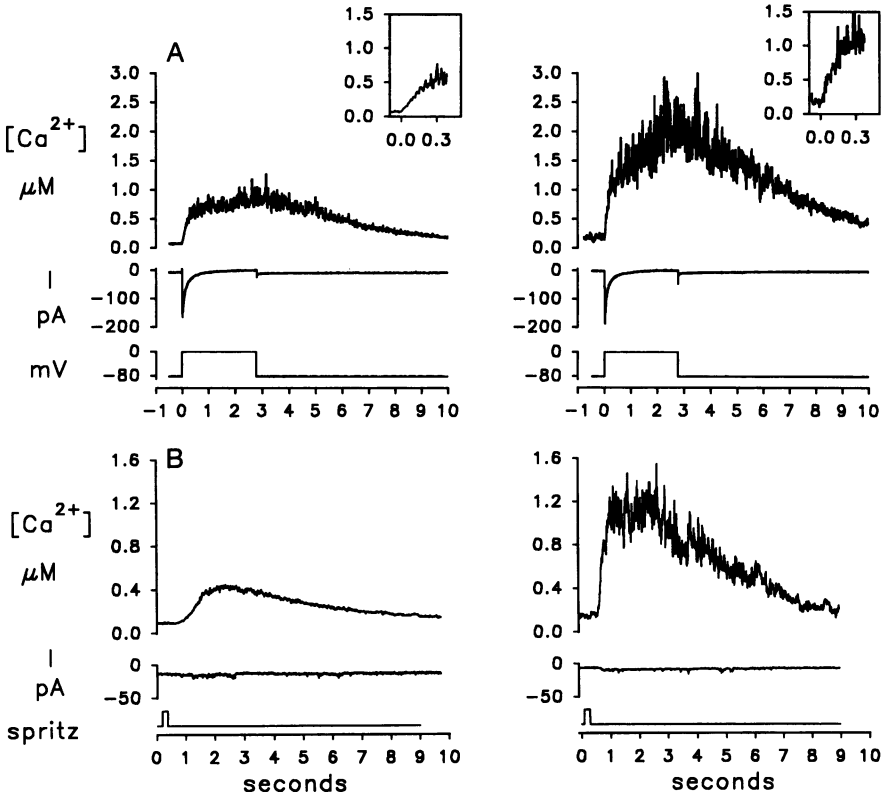

FIG. 3. Comparison of the $[Ca^{2+}]_i$ transients recorded using fura-2 and FFP18. (*A*) Changes in $[Ca^{2+}]_i$ recorded using either fura-2 (*Left*) or FFP18 (*Right*), and the inward Ca^{2+} current that occurred in response to a 3-sec membrane depolarization from −80 to 0 mV. The peak inward current in these two cells is similar, indicating that the amount of Ca^{2+} entering across the plasma membrane was the same. $[Ca^{2+}]_i$ records were smoothed once using a three-point running average. Parameter values used to calculate $[Ca^{2+}]$ were as follows: for fura-2, R_{max} = 19.3, R_{min} = 0.52, β = 13.3, and K_d = 200 nM; for FFP18, R_{max} = 6.0, R_{min} = 0.35, β = 8.0, and K_d = 400 nM. (*Insets*) First 300 msec of $[Ca^{2+}]_i$ transients (not smoothed) that were fit by a single exponential function to determine the initial rate of rise. (*B*) Changes in $[Ca^{2+}]_i$ recorded using either fura-2 (*Left*) or FFP18 (*Right*), and membrane current that occurred after a 200-msec extracellular application of 20 mM caffeine by pressure ejection from a broken-tipped pipette placed close to the cell. Membrane potential was held at −80 mV, and there was no significant caffeine-activated inward cation current. Parameters were as follows: for fura-2, R_{max} = 17, R_{min} = 0.4, β = 15, and K_d = 200 nM; for FFP18, R_{max} = 6.0, R_{min} = 0.35, β = 8.0, and K_d = 400 nM. The rate of rise was measured by fitting a straight line or a single exponential function to the first 300 msec or (to avoid effects of possible interaction of caffeine with the indicator) to the 300 msec after the initial foot.

experiments did not, however, introduce errors into our $[Ca^{2+}]_i$ estimates that affect our conclusions.§

To see how FFP18 distributes inside cells and what intracellular membranes it associates with we obtained three-dimensional images of FFP18 inside smooth muscle cells. An image in a selected plane transecting the center of the cell (Fig. 2*A*) shows that most intracellular FFP18 associated with the plasma membrane or membraneous structures very close to it. FFP18 also associates with the nuclear membrane. Fig. 2*B* shows that the fluorescence at the center of the loaded cell is above the autofluorescence level in that cell, indicating that some FFP18 is free or associated with unresolvable structures away from the cell surface. Analysis of cross-sections of three-dimensional images indicated that at least 65% of the FFP18 fluorescence inside cells (where FFP18 had diffused into the cell for 15–20 min) was located in a thin annulus (≈1 μm wide) containing the surface membrane and closely adjacent structures. Images at the cell surface (Fig. 2*C*) reveal the indicator to be distributed inhomogeneously. Previous immunocytochemical studies (37) have shown that much of the SR of these smooth muscle cells is located close to the plasma membrane and that the membrane is composed of two domains: one containing several different ion transporters in close apposition to elements of the SR and another enriched in cytoskeletal attachment proteins. Thus, while FFP18 is principally associated with structures near the cell surface, it is nonuniformly distributed there: FFP18 appears to be localized on specific domains of the plasma membrane and/or membranes of the peripheral SR. In contrast, cells loaded with fura-2 (free acid) show a mottled fluorescence cloud. There are dim regions and bright regions, which may represent exclusion from or concentration between organelles, but the locally averaged fluorescence intensity is similar throughout the cell.

To explore the possibility that $[Ca^{2+}]_i$ directly beneath the cell membrane might change differently than $[Ca^{2+}]_i$ in the bulk cytosol during Ca^{2+} influx through voltage-gated Ca^{2+} channels, we recorded $[Ca^{2+}]_i$ changes that occur in response to membrane depolarization using both FFP18 and fura-2. We simultaneously recorded the inward Ca^{2+} current and compared the time course of the $[Ca^{2+}]_i$ transients recorded using FFP18 to those recorded using fura-2 in cells where the peak amplitude of the inward current was the same. Typical results from two cells are shown in Fig. 3*A*. The FFP18-recorded $[Ca^{2+}]_i$ transient rises from resting level (≈200 nM) to 1 μM within the first 200 msec and then continues to rise slowly until membrane repolarization. In contrast, the fura-2-recorded $[Ca^{2+}]_i$ transient rises more slowly, reaching only 500 nM in the first 200 msec. The initial resting $[Ca^{2+}]$ level in cells measured by FFP18 (172 ± 11 nM, n = 9) was slightly higher than the resting $[Ca^{2+}]$ levels measured by fura 2 (117 ± 27 nM, n = 8). (All numbers indicate mean ± SEM, n = number of cells). The initial rate of rise of the $[Ca^{2+}]_i$ transients recorded using FFP18 (5.23 ± 1.2 μM/sec, peak I_{Ca} = 122 ± 13 pA, n = 7) was 3.25 times greater than the initial rate of rise of $[Ca^{2+}]_i$ transients recorded using fura-2 (1.61 ± 0.37 μM/sec, peak I_{Ca} = 123 ± 3 pA, n = 9). Also, the FFP18-recorded $[Ca^{2+}]_i$ transients rose to higher $[Ca^{2+}]$ levels (1.11 ± 0.19 μM) than the fura-2-recorded $[Ca^{2+}]_i$ transients (0.63 ± 0.08 μM). The FFP18 records indicate that early during Ca^{2+} influx, $[Ca^{2+}]_i$ near the plasma membrane reaches levels at least two times higher than the cytoplasmic $[Ca^{2+}]_i$ reported by fura-2 at that time.

To learn about near-membrane and cytoplasmic $[Ca^{2+}]$ changes that occur when Ca^{2+} is released from internal Ca^{2+} stores, we recorded Ca^{2+} transients using FFP18 or fura-2 in response to caffeine. Caffeine causes Ca^{2+} release from the SR through ryanodine-sensitive Ca^{2+}-release channels in these smooth muscle cells (38). To study $[Ca^{2+}]_i$ changes due only to SR Ca^{2+} release, we selected cells that did not contain any caffeine-activated nonselective cation current or applied caffeine at a membrane holding potential of +60 mV, where the cation current

§For example, if the FFP18 concentration during an experiment were high (a concentration corresponding to the highest density acheived for FFP18 applied to the outside of cells) and the concentration used in calibration were four times lower (lowest concentration used for calibrations), then the calculated $[Ca^{2+}]_i$ would underestimate the true $[Ca^{2+}]_i$, in the nanomolar or micromolar range, by 20–30%. This error is small in comparison to the 5-fold increases in $[Ca^{2+}]_i$ observed upon cell stimulation.

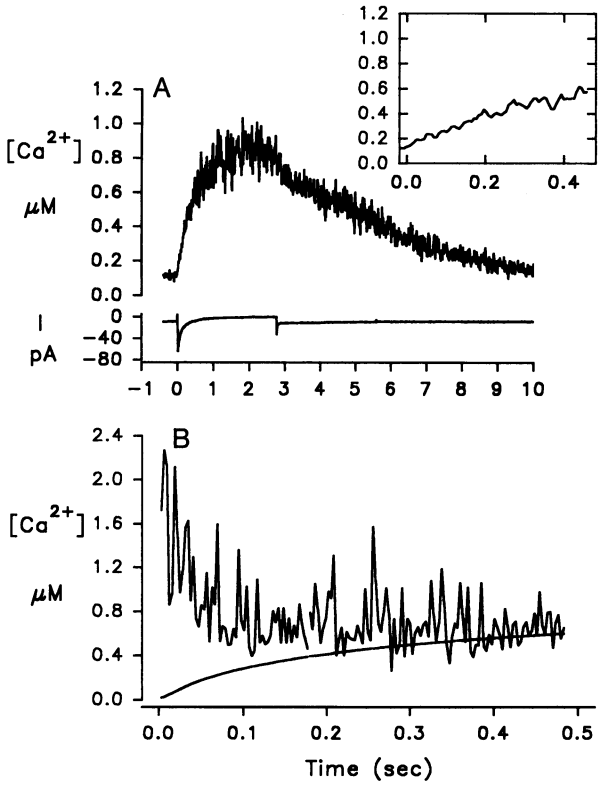

FIG. 4. Estimates of near-membrane and cytosolic components of a $[Ca^{2+}]_i$ transient recorded during membrane depolarization using FFP18. (*A*) $[Ca^{2+}]_i$ transient recorded using FFP18 and membrane current that occurred in response to a 3-sec depolarization from −80 to 0 mV. (*Inset*) First 500 msec of the $[Ca^{2+}]_i$ transient. (*B*) Calculated components of the first 500 msec of the $[Ca^{2+}]_i$ transient shown in *A*. The smooth line shows the cytosolic component, and the noisier line shows the calculated near-membrane component.

is outward and no $[Ca^{2+}]_i$ increase occurs after opening of these nonselective channels (38). Typical results are shown in Fig. 3*B*. The FFP18-recorded transients rose 15 times faster ($d[Ca^{2+}]/dt_{max}$ = 4.22 ± 1.2 μM/sec, n = 4) than the fura-2-recorded transients ($d[Ca^{2+}]/dt_{max}$ = 0.27 ± 0.07, n = 3). Also, the $[Ca^{2+}]_i$ transients recorded using FFP18 rose to higher levels (0.81 ± 0.08 μM) than the $[Ca^{2+}]_i$ transients recorded using fura-2 (0.29 ± 0.05 μM). The much faster kinetics of the FFP18-recorded, caffeine-induced $[Ca^{2+}]_i$ transients suggest that FFP18 was localized near sites of SR Ca^{2+} release. This possibility is supported by images of the distribution of intracellular FFP18 near the cell membrane (Fig. 2*C*).

The difference between the peak rates of rise of FFP18-recorded $[Ca^{2+}]_i$ transients and fura-recorded $[Ca^{2+}]_i$ transients induced by caffeine (15 times) is much greater than the difference for depolarization-induced $[Ca^{2+}]_i$ transients (3.5 times). The rates of rise of FFP18-recorded transients are similar, whether induced by caffeine (4.2 μM/sec) or membrane depolarization (5.2 μM/sec), whereas the caffeine-induced $[Ca^{2+}]_i$ transients recorded by fura-2 are much slower rising than depolarization-induced transients recorded by fura-2. These observations might be explained if Ca^{2+} were released from the SR into a restricted space such that it mixed less readily with the bulk cytoplasm than such Ca^{2+} entering through voltage-gated channels on the plasma membrane.

The $[Ca^{2+}]_i$ transient recorded using fura-2 during membrane depolarization rises rapidly when the magnitude of the inward current is large and then continues to rise slowly for some time as Ca^{2+} continues to enter the cell and diffuses into the bulk cytoplasm. The $[Ca^{2+}]_i$ near the plasma membrane, recorded using FFP18, rises even higher during the peak of inward Ca^{2+} current, but then when the Ca^{2+} influx rate declines, the near-membrane $[Ca^{2+}]_i$ would be predicted to fall as Ca^{2+} diffuses away from the membrane and is pumped out of the cell. The continuous rise in the FFP18-recorded $[Ca^{2+}]_i$ transients throughout depolarization, similar to the rise of the fura-2-recorded transients, suggests that the FFP18-recorded transient may be a mixture of signals from the plasma membrane and the surrounding cytoplasm. This hypothesis is supported by our images of FFP18 distribution (Fig. 2) that reveal a small but finite fraction of the dye located away from the cell membrane. We used our image analysis as a basis for mathematically dissecting the FFP18-recorded $[Ca^{2+}]_i$ transients into near-membrane and cytoplasmic components to better estimate the time course of changes in near-

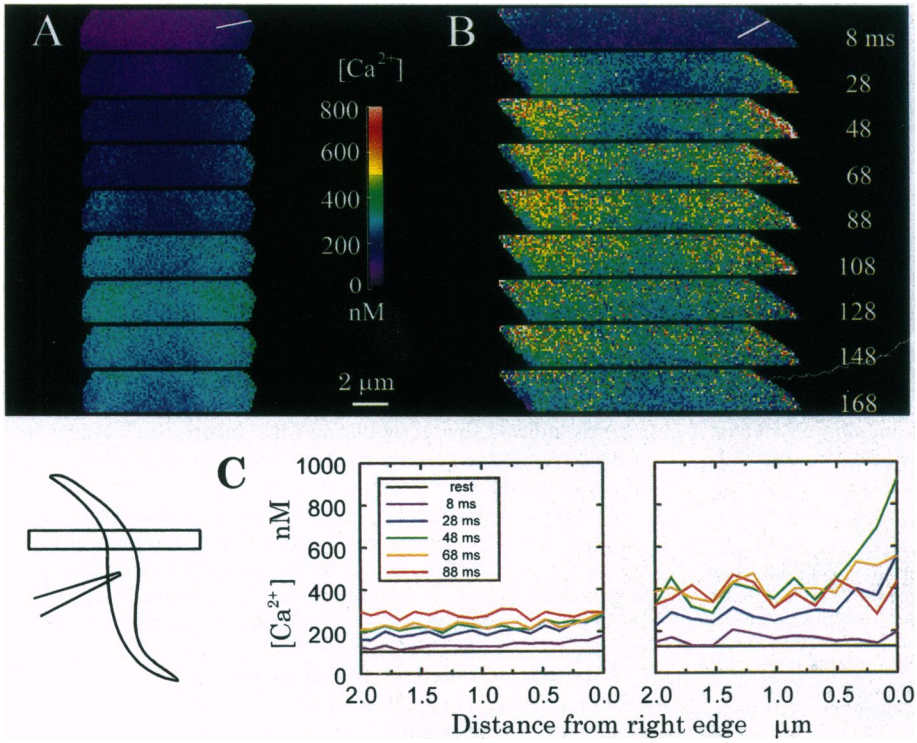

FIG. 5. Series of images of $[Ca^{2+}]_i$ measured using fura-2 or FFP18 at the indicated times (far right) during depolarization from −80 to 0 mV in two patch-clamped cells with similar peak inward Ca^{2+} currents. The patch-clamped cell, as shown at lower right, crossed the narrow image field with the tip of the patch-pipette outside of the image field. Thus, images show a short segment of the cell, focused on a central plane, so that the membranes are most in focus on either side. (*A*) Patch-pipette solution contained 50 μM fura-2. Peak inward current was 93 pA. Parameters used to calculate $[Ca^{2+}]$ were as follows: R_{max} = 17.7, R_{min} = 1.4, β = 6.2, K_d = 200 nM. (*B*) Pipette solution contained 30 μM FFP18 and 50 μM EGTA. Peak inward current was 80 pA. R_{max} = 8.0, R_{min} = 1.34, β = 3.7, K_d = 400 nM. (*C*) Plots of $[Ca^{2+}]_i$ along a line (see white lines on images at 8 ms) drawn from the right edge toward the center of the cell in each fura-2-recorded image in *A* (*Left*) or FFP18-recorded image in *B* (*Right*). Black curves (rest) are from images taken before depolarization (data not shown). $[Ca^{2+}]_i$ values are an average from three pixels: one pixel on the line and one on either side of it.

membrane $[Ca^{2+}]_i$ in these cells. Fig. 4*B* shows the result of dissecting one $[Ca^{2+}]_i$ transient in this way, assuming that 65% of the signal came from the surface membranes and 35% came from the cytoplasm. The near-membrane $[Ca^{2+}]_i$ rose to micromolar levels upon depolarization and then declined rapidly toward the final $[Ca^{2+}]_i$ in the cytoplasm. $[Ca^{2+}]_i$ in the cytoplasm rose much more slowly and gradually toward this final level. $[Ca^{2+}]_i$ transients from three other cells were analyzed in this way with similar results.

Our mathematical analysis suggested that there was a much briefer, large near-membrane $[Ca^{2+}]_i$ signal not being detected by monitoring FFP18 fluorescence from the whole cell. To more directly isolate the near-membrane signal we imaged intracellular FFP18 fluorescence in a stimulated cell and then calculated the $[Ca^{2+}]$ changes at the cell membrane. Fig. 5 shows a series of images of $[Ca^{2+}]_i$ reported by fura-2 in one cell (Fig. 5*A*) and by FFP18 in another cell (Fig. 5*B*) at 20-msec intervals during membrane depolarization that evoked similarly small inward Ca^{2+} currents. As evident, the $[Ca^{2+}]_i$ reported by FFP18 at the cell membrane rises above the resting level within the first 20 msec, peaks within 50 msec [time to peak ranged from 40 to 100 ms (mean 81.3 ± 11.8, $n = 6$)], and then slowly declines. The $[Ca^{2+}]_i$ reported by fura-2 rises more slowly and continues to rise throughout the time images were acquired ($n = 6$). The graphs in Fig. 5*C* show changes in the radial distribution of $[Ca^{2+}]_i$ within 2 μm of the cell membrane during the first 100 msec of depolarization. Fig. 5*C Right* shows that, in the FFP18-recorded images, a $[Ca^{2+}]_i$ gradient between the membrane and the cytoplasm develops, is steepest at 48 ms (green curve), and then collapses. Fig. 5*C Left* shows that such $[Ca^{2+}]_i$ gradients are not apparent in the fura-2-recorded images.

There is a ryanodine-sensitive component of $[Ca^{2+}]_i$ transients, recorded using fura-2, in gastric smooth muscle in response to membrane depolarization (39), suggesting that the rise in $[Ca^{2+}]_i$ induced by membrane depolarization includes a Ca^{2+} influx-induced release of Ca^{2+} from the SR through ryanodine-sensitive SR Ca^{2+} channels. The appearance of this component at times (100–200 msec after depolarization) when the $[Ca^{2+}]_i$ measured by fura-2 was <500 nM made it difficult to explain how this mechanism could occur in these cells because this mechanism, when studied out of the intact cell, requires a $[Ca^{2+}]$ exceeding micromolar levels to be activated (5, 9). The $[Ca^{2+}]_i$ transients recorded using FFP18 indicate that near-membrane $[Ca^{2+}]_i$ rises to micromolar levels within the first 200 msec after membrane depolarization. These high $[Ca^{2+}]_i$ levels and rapid rates of $[Ca^{2+}]_i$ increase are more likely to activate SR Ca^{2+} release in these cells. These large changes in near-membrane $[Ca^{2+}]_i$ could also activate Ca^{2+}-activated K^+ currents (11, 12) and evoke significant Ca^{2+} extrusion through the Na^+/Ca^{2+} exchanger (10) in these cells.

The $[Ca^{2+}]_i$ measured at the membrane in these images rose and diffused away rapidly but did not reach $[Ca^{2+}]_i$ levels as high as predicted by our mathematical analysis of the FFP18-recorded $[Ca^{2+}]_i$ transients (Fig. 4) or by models of the $[Ca^{2+}]_i$ changes near the mouth of Ca^{2+} channels during Ca^{2+} influx (15, 16). There are several possible reasons for this. The fluorescent signal at the membrane may represent a mixture of signals from the plasma membrane and from the surrounding cytoplasm. These images of fluorescence inside relatively thick cells (6- to 10-μm diameter) were obtained using a wide-field microscope and were not processed to remove out-of-focus information; therefore fluorescence from neighboring regions of the cell contributed to the signal measured at the cell membrane. The $[Ca^{2+}]_i$ signal at the membrane may also be attenuated because exposure times at each wavelength, although quite short, were still long relative to rapid changes in $[Ca^{2+}]_i$. In addition, as with other Ca^{2+} indicators, when FFP18 is highly concentrated, it may buffer the near-membrane $[Ca^{2+}]$ transient. Membrane-associating Ca^{2+} indicators that have lower Ca^{2+} affinity, have fast Ca^{2+}-binding kinetics, and are brighter would improve our ability to measure large $[Ca^{2+}]_i$ changes. In spite of present limitations, FFP18 represents a significant step in our ability to measure localized Ca^{2+} signals. We have recorded large, rapid, more-transient changes in $[Ca^{2+}]_i$ with FFP18 that provide additional insights into the time course of $[Ca^{2+}]_i$ changes near the plasma membrane and help us understand how membrane processes in smooth muscle are regulated by $[Ca^{2+}]_i$.

We acknowledge Richard A. Tuft for continuous development of the high-speed digital imaging system, Douglas S. Bowman for development of special software for these experiments, and Jeffrey Carmichael and Kristine Perry for isolation of smooth muscle cells. This work was supported by grants GM14157 (E.F.E.), GM40605 (M.P.), and HL 14523 (F.S.F.) from the National Institutes of Health and 9022325 (M.P.) and BIR-9200027 (F.S.F.) from the National Science Foundation.

1. Becker, P. L., Singer, J. J., Walsh, J. V., Jr., & Fay, F. S. (1989) *Science* **244,** 211–214.
2. Vivadou, M. B., Singer, J. J. & Walsh, J. V., Jr. (1991) *Pflügers Arch.* **418,** 144–152.
3. Missiaen, L., Wuytack, F., Raeymaekers, L., DeSmedt, H., Droogmans, G., Declerck, I. & Casteels, R. (1991) *Pharmacol. Ther.* **50,** 191–232.
4. Herrmann-Frank, A., Edward, D. & Meissner, G. (1990) *Pflügers Arch.* **418,** 353–359.
5. Xu, F., Lai, A., Cohn, A., Etter, E., Guerrero, A., Fay, F. & Meissner, G. (1994) *Proc. Natl. Acad. Sci. USA* **91,** 3294–3298.
6. Somlyo, A. V., Bond, M., Somlyo, A. P. & Scarpa, A. (1985) *Proc. Natl. Acad. Sci. USA* **82,** 5231–5235.
7. Albritton, N. L., Meyer, T. & Stryer, L. (1992) *Science* **258,** 1812–1815.
8. Sala, F. & Hernandez-Cruz, A. (1990) *Biophys. J.* **57,** 313–324.
9. Iino, M. (1989) *J. Gen. Physiol.* **94,** 363–383.
10. Blaustein, M., DiPolo, P. R. & Reeves, J. P. (1991) *Ann. N.Y. Acad. Sci.* **639,** 482–575.
11. Singer, J. J. & Walsh, J. V., Jr. (1987) *Pflügers Arch.* **408,** 98–111.
12. Gurney, A. M., Tsien, R. Y. & Lester, H. A. (1987) *Proc. Natl. Acad. Sci. USA* **84,** 3496–3500.
13. Gunter, T. E. & Pfeiffer, D. R. (1990) *Am. J. Physiol.* **258,** C755–C786.
14. Stern, M. D. (1992) *Cell Calcium* **13,** 183–192.
15. Simon, S. M. & Llinas, R. R. (1985) *Biophys. J.* **48,** 485–498.
16. Fogelson, A. L. & Zucker, R. S. (1985) *Biophys. J.* **48,** 1003–1017.
17. Kargacin, G. J. (1994) *Biophys. J.* **67,** 262–272.
18. Hume, J. R. & LeBlanc, N. (1989) *J. Physiol. (London)* **413,** 49–73.
19. Lederer, W. J., Niggli, E. & Hadley, R. W. (1990) *Science* **248,** 283.
20. Wier, W. G., Egan, T. M., Lopez-Lopez, J. R. & Balke, C. W. (1994) *J. Physiol. (London)* **474,** 463–471.
21. Benham, C. D. & Bolton, T. B. (1986) *J. Physiol. (London)* **381,** 385–406.
22. Neher, E. & Augustine, G. J. (1992) *J. Physiol. (London)* **450,** 273–301.
23. Hernandez-Cruz, A., Sala, F. & Adams, P. R. (1990) *Science* **247,** 858–861.
24. Llinas, R. R., Sugimori, M. & Silver, R. B. (1992) *Science* **256,** 677–679.
25. Etter, E. F., Kuhn, M. A. & Fay, F. S. (1994) *J. Biol. Chem.* **269,** 10141–10149.
26. Fay, F. S., Hoffman, R., LeClair, S. & Merriam, P. (1982) *Methods Enzymol.* **85,** 284–292.
27. Yagi, S., Becker, P. L. & Fay, F. S. (1988) *Proc. Natl. Acad. Sci. USA* **85,** 4109–4113.
28. Grynkiewicz, G., Poenie, M. & Tsien, R. Y. (1985) *J. Biol. Chem.* **260,** 3440–3450.
29. Loew, L. M., Tuft, R. A., Carrington, W. & Fay, F. S. (1993) *Biophys. J.* **65,** 2396–2407.
30. Carrington, W. A. (1990) *Proc. SPIE* **1205,** 72–83.
31. Isenberg, G., Etter, E., Wendt-Gallitelli, M.-F., Schiefer, A., Carrington, W., Tuft, R. & Fay, F. (1996) *Proc. Natl. Acad. Sci. USA* **93,** in press.
32. Guerrero, A., Singer, J. J. & Fay, F. S. (1994) *J. Gen. Physiol.* **104,** 395–422.
33. Becker, P. L. & Fay, F. S. (1987) *Am. J. Physiol.* **253,** C613–C618.
34. Vorndran, C., Minta, A. & Poenie, M. (1995) *Biophys. J.* **69,** 2112–2124.
35. Sims, P. J., Waggoner, A. S., Wang, C.-H. & Hoffman, J. F. (1974) *Biochemistry* **13,** 3315–3330.
36. Lakowicz, J. R. (1983) *Principles of Fluorescence Spectroscopy* (Plenum, New York), pp. 257–270.
37. Moore, E. D., Etter, E. F., Phillipson, K. D., Carrington, W. A., Fogarty, K. E., Lifshitz, L. M. & Fay, F. S. (1993) *Nature (London)* **365,** 657–660.
38. Guerrero, A., Fay, F. S. & Singer, J. J. (1994) *J. Gen. Physiol.* **104,** 375–394.
39. Guerrero, A., Kirber, M. T., Singer, J. J. & Fay, F. S. (1993) *Biophys. J.* **64,** A153 (abstr.).